Mechanism of Charge Transport along Columnar Stacks of a Triphenylene Dimer

ARTICLE *in* THE JOURNAL OF PHYSICAL CHEMISTRY B · NOVEMBER 1998

Impact Factor: 3.3 · DOI: 10.1021/jp9828989

Mechanism of Charge Transport along Columnar Stacks of a Triphenylene Dimer

Anick M. van de Craats,[†] Laurens D. A. Siebbeles,*[,†] Ingo Bleyl,[‡] Dietrich Haarer,[‡] Yuri A. Berlin,[†,§] Anatoly A. Zharikov,[§] and John M. Warman[†]

IRI, Radiation Chemistry Department, Delft University of Technology, Mekelweg 15, 2629 JB Delft, The Netherlands, Lehrstuhl Experimentalphysik IV and Bayreuther Institut für Makromolekülforschung (BIMF), Universität Bayreuth, D-95440 Bayreuth, Germany, and Technische Universität München, Physik Department T-38, D-85748 München, Germany

Received: July 7, 1998; In Final Form: September 25, 1998

We have measured the mobility of charge carriers along the one-dimensional conducting pathways provided by columnar stacks of triphenylene units in the liquid crystalline dimer 1,10-di-[3′,6′,7′,10′,11′-pentabutyloxytriphenylenyl-2-oxy]decane using the pulse-radiolysis time-resolved microwave conductivity (PR-TRMC) and the time-of-flight (TOF) techniques. The high frequency (30 GHz) and TOF intracolumnar mobilities approach the same value (ca. 0.01 $cm^2\ V^{-1}\ s^{-1}$) at the highest temperatures studied (about 400 K). When the temperature is lowered, the high-frequency mobility remains almost constant within the range $(1.5 \pm 0.5) \times 10^{-2}\ cm^2\ V^{-1}\ s^{-1}$ down to 170 K. The value of μ_{TOF} in contrast decreases dramatically at lower temperatures, reaching a value as low as $2 \times 10^{-6}\ cm^2\ V^{-1}\ s^{-1}$ at 130 K. The different temperature dependences found are attributed to structural disorder within the columnar stacks. The experimental data are compared with predictions of the influence of static disorder on charge transport using different transport models. Our analytical and computer simulation studies show that the only transport mechanism consistent with both sets of experimental data is one involving thermally activated jumps over barriers with an exponential distribution of barrier heights. The experimental mobility values could be reproduced with a mean barrier height of 0.024 eV and an attempt frequency for jumping equal to 1 ps^{-1}. Our experimental and theoretical findings illustrate the added insights into the underlying mechanism of charge transport in complex molecular materials that can be gained from the combined results of TOF and high-frequency mobility measurements.

1. Introduction

Peripherally hexaalkoxy-substituted triphenylenes belong to the class of discotic organic molecules that are characterized by a flat aromatic core to which several alkyl chains are attached. Such discotic molecules self-organize into columnar stacks of the aromatic cores surrounded by an insulating saturated hydrocarbon mantle.[1] The columns provide one-dimensional (1-D) pathways for rapid charge[2−4] and energy migration.[5] The possibility of a rapid, channeled transport in combination with the ability of discotic materials to form liquid crystalline phases makes them interesting candidates for applications in photocopying, electrophotography, nonlinear optics, and molecular electronics.[6−9]

One of the main factors affecting the charge transport properties of liquid crystalline discotic materials is expected to be positional disorder, i.e., the nonparallel arrangement of disks and longitudinal and lateral displacements of molecular cores within the stacks.[10] Deviations from ideal stacking will lead to energy disorder and temporary charge localization. As a result, charge transport along the 1-D pathway becomes incoherent and proceeds by successive transitions from one localization site to another.

Theoretically the incoherent jumplike motion is treated as the random walk of a particle in a rough potential energy profile (for a review, see refs 11−13 and references therein). Several analytical approaches[14−17] and the Monte Carlo simulation technique enable one to study the 1-D motion for different model profiles (a smooth potential locally perturbed by random traps and/or random barriers) and for various mechanisms of site-to-site transitions (thermally activated jumps or tunneling).[18−27] In all cases the net result of 1-D energy disorder has been shown to be a sublinear dependence of the mean-square displacement on time. Consequently, the incoherent 1-D transport becomes non-Gaussian, i.e., dispersive. A similar effect is known for three-dimensional systems[14,28−31] (for comparison of 1-D and 3-D systems see ref 21).

A question that arises is whether existing dispersive transport theories can quantitatively describe intracolumnar charge carrier motion in discotic liquid crystals. One of the greatest difficulties in answering this question lies in the fact that up to now only very limited mobility data over a very narrow temperature range have been available for these materials.[2,4,32−36] The width of the temperature range accessible for the measurements is often restricted by the thermal stability of the mesophase and usually does not exceed 50° in the case of monomeric triphenylene derivatives. Exceptions are dimeric triphenylene derivatives, which exhibit a liquid crystalline phase over much wider temperature intervals from just below their melting points at close to 400 K down to at least 130 K.[10,37]

This property is utilized in the present work to study charge carrier mobilities over a large temperature range in the liquid crystalline triphenylene dimer 1,10-di-[3′,6′,7′,10′,11′-pentabutyloxytriphenylenyl-2-oxy]decane (hereafter referred to simply

* Corresponding author. E-mail: siebbel@iri.tudelft.nl. Fax: ++31 15 2787421.
† Delft University of Technology.
‡ Universität Bayreuth.
§ Technische Universität.

10.1021/jp9828989 CCC: $15.00
Published on Web 11/10/1998

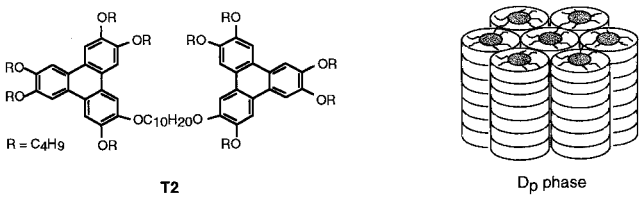

Figure 1. Molecular structure of 1,10-di-[3′,6′,7′,10′,11′-pentabutyloxytriphenylenyl-2-oxy]decane, T2, and a schematic representation of its columnar liquid crystalline plastic D_p phase.

as T2). The primary molecular structure consists of two pentabutyloxy-substituted triphenylene cores connected via a long oxydecyloxy spacer as shown in Figure 1. Similar to other triphenylenes, T2 forms columnar stacks of triphenylene units with the stacks arranged in a two-dimensional hexagonal array.

Two different experimental techniques, namely, the time-of-flight (TOF) and pulse-radiolysis time-resolved microwave conductivity (PR-TRMC) methods, have been used to determine the mobility of charge carriers. In the former, a constant voltage is used and the transit time of the carriers between two parallel electrodes is measured. In the latter a rapidly oscillating (30 GHz) electric field is used to probe the charge carrier motion without the necessity of electrodes. The experimental results are compared with those from different theoretical charge transport models, which provides insight into the mechanism of charge transport in the material studied.

The paper is organized as follows. Section 2 describes the material studied and the experimental techniques used for the mobility measurements. The models exploited in the theoretical analysis and the methodology of the computer simulations are discussed in section 3. The results of experiment and theory are compared in section 4. The conclusions are summarized in section 5.

2. Experimental Section

2.1. Material. The synthesis of T2 was analogous to that previously reported for the triphenylene complex with peripheral pentyloxy side chains.[37] T2 was found to form a plastic discotic phase, D_p,[27] observed also for the butyloxy monomer 2,3,6,7,-10,11-hexabutyloxytriphenylene.[34,38] As inferred from X-ray data, the D_p phase exhibits long-range hexagonal order (see Figure 1). The intracolumnar order is higher than in a typical D_h phase, and the distance between adjacent disks is 3.5 Å.[10,27,34,38] Rotation of the triphenylene cores around the columnar axis is hindered because of the spacer, as was shown for a pentyloxy analogue by NMR.[10] A clear-cut phase transition in a DSC scan was found at 421 K, corresponding to melting to the isotropic liquid phase.

2.2. Mobility Measurements. The charge carrier mobility in T2 was measured by PR-TRMC and TOF techniques, which have been described in detail in refs 36, 39−41, and 42, respectively (for comparison of the two methods, see refs 4 and 36). In the two subsections below the methods to obtain mobilities using the PR-TRMC and TOF techniques are presented.

2.2.1. Pulse-Radiolysis Time-Resolved Microwave Conductivity (PR-TRMC) Method. An amount of 165 mg of the dimer was compressed into a rectangularly shaped microwave reflection cell of cross-section 7.1 × 3.55 mm^2 and length 14 mm. The cell was irradiated with a 20 ns, 4 A pulse of 3 MeV electrons from a van de Graaff accelerator. The integrated beam charge per pulse, Q (in nC), was monitored routinely and was on the order of 80 nC for the pulses used. The primary high-energy electrons lose approximately 20% of their energy during penetration of the sample, resulting in a close to uniform spatial distribution of ionization events.[40] The energy deposited in the sample per unit volume and per unit beam charge, D/Q (in J m^{-3} nC^{-1}), was accurately determined by dosimetry and was equal to 1080 J m^{-3} nC^{-1}. The mean energy required to produce one electron−hole pair, E_p (in eV), is expected to be similar to that found for other hydrocarbon media, i.e., approximately 25 eV.[43−45] The initial concentration of ionization events, $N_p(0) = Q[D/Q]/(eE_p)$, for the pulse conditions used was therefore approximately 2×10^{22} m^{-3} or 40 μM. The accumulated radiation dose used in the present experiments was orders of magnitude lower than that required to influence the magnitude or decay kinetics of the conductivity transients.[40]

The radiation-induced conductivity of the sample, $\Delta\sigma$, resulting from the formation of mobile charge carriers, was monitored with nanosecond time resolution as a change in the microwave power absorbed by the sample. The microwave frequency band used was 28−39 GHz. For small changes in conductivity, the relative change of the microwave power, $\Delta P/P$, is directly proportional to $\Delta\sigma$, and the proportionality factor can be calculated as described previously.[46] Typical conductivity transients, taken on a linear time scale for the first 150 ns and on a logarithmic time scale for times from 10 ns to 1 ms, are shown in Figure 2. The transients are characterized by an initial rapid decay over the first few nanoseconds followed by a much slower decay. In the present work we will be mainly concerned with the end-of-pulse conductivity per unit dose absorbed, $\Delta\sigma_{eop}/D$ (in S m^2/J), which is taken as the magnitude of the slowly decaying component immediately following the pulse, as illustrated in Figure 2A.

As shown previously,[4,36,41] the sum of the positive and negative charge carrier mobilities, $\sum\mu_{PR-TRMC} = \mu_+ + \mu_-$, can be derived from $\Delta\sigma_{eop}/D$ using the relationship

$$\sum\mu_{PR-TRMC} = [\Delta\sigma_{eop}/D]E_p/F_{eop} \qquad (1a)$$

In eq 1a F_{eop} is the fraction of initially formed charge carrier pairs that survive rapid geminate recombination during the pulse. The value of F_{eop} was calculated to be 0.42 using the method presented in ref 47. In TRMC experiments the organized columnar domains are oriented randomly in the bulk material. For each domain, charge transport is expected to occur preferentially along the columnar axis.[4,41,48,49] Hence, the mean value of the mobility averaged over all orientations, $\sum\mu_{PR-TRMC}$, is related to the one-dimensional, intracolumnar mobility, $\sum\mu_{1d}$, by

$$\sum\mu_{1d} = 3\sum\mu_{PR-TRMC} \qquad (1b)$$

It is therefore this latter parameter that should be compared with the time-of-flight mobility, since in TOF measurements the columns are all considered to be stacked orthogonally to the surface of the electrodes, i.e., parallel to the applied electric field.

2.2.2 Time-of-Flight (TOF) Method. In the TOF experiments the material was placed in a cell consisting of two aluminum-coated semitransparent glass plates, which are separated by spacers to 31.2 μm. In contrast to the PR-TRMC method, charge carriers are generated in a constant electric field by illumination with a short laser pulse (nitrogen laser with 337 nm, 10 ns pulse length, 10 mJ). The pulse energy was reduced to avoid space charge effects. Owing to the small penetration depth of the incident laser light, charge carriers are formed only in the thin layer at the front electrode. The transport of the charge carriers in the applied electric field to the counter

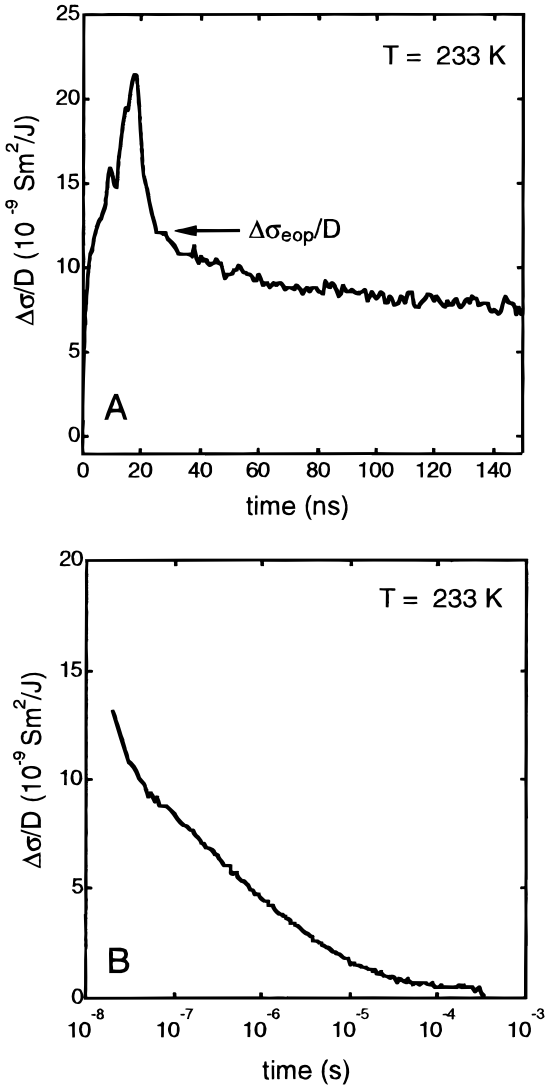

Figure 2. Examples of PR-TRMC transients obtained on pulsed irradiation of T2 at a temperature of 233 K: (A) displayed on a linear time scale for the first 150 ns after the pulse; (B) displayed on a logarithmic time scale for elapsed times between 10 ns and 1 ms.

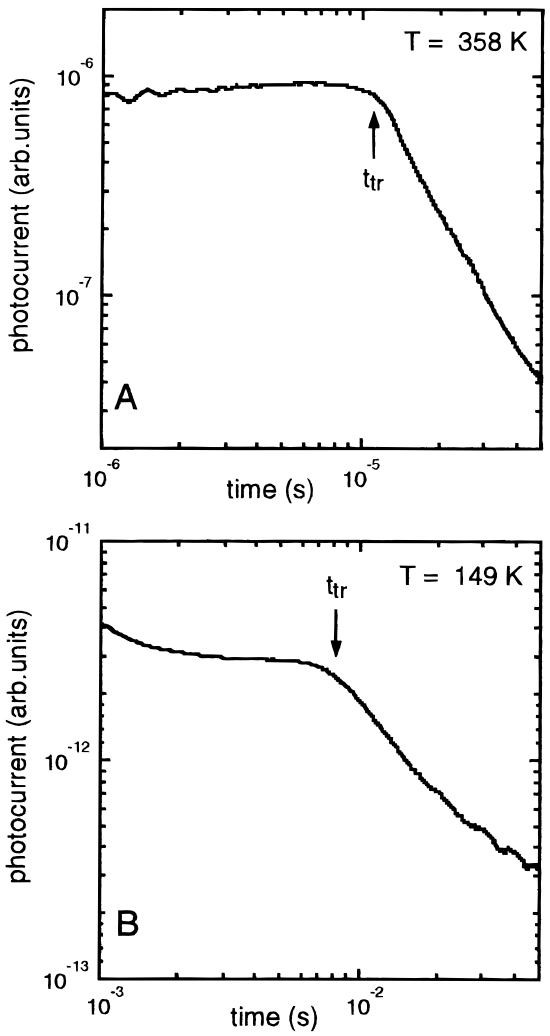

Figure 3. Typical photocurrent transients recorded for the triphenylene dimer T2 at 358 K (A) and 149 K (B) for an interelectrode distance of 31.2 μm and an applied potential difference of 100 V.

electrode induces a displacement current, which can be detected with a current amplifier and a storage oscilloscope. The TOF setup has been described in greater detail elsewhere.[42]

Examples of photocurrent transients are shown plotted in a double-logarithmic representation in Figure 3. Such transients can be approximated by two linear components with different slopes at short and long times. The transit time t_{tr} is defined as the time where these lines intersect.[14,29] The mobility of the charge carriers, μ_{TOF}, can be calculated from t_{tr} as follows

$$\mu_{TOF} = L^2/(Vt_{tr}) \tag{2}$$

where L is the sample thickness and V is the applied voltage.

3. Theoretical

3.1. Transport Models. A realistic model of one-dimensional charge carrier transport in columnar discotic liquid crystals should take account of positional disorder along the columnar stacks of the central aromatic units.[10] Such disorder causes the interaction between adjacent aromatic disks to fluctuate and therefore to give rise to 1-D energy disorder. This can be approximated by potential energy profiles with wells of random energy depths and/or barriers with random energy heights. Let us assume that at the initial instant of time a charge carrier is temporarily localized either in one of these wells or between adjacent random barriers and that afterward it is able to undergo successive transitions between neighboring sites. The task is then to describe the resulting 1-D motion of charge carriers in terms of the mobility, i.e., the net distance traveled in unit time in unit applied field.

To reach this goal, the explicit form of the transition rate between neighboring localization sites must be specified. This can be done by invoking different theoretical models,[18−27] schematically illustrated in Figure 4. These can differ in the shape postulated for the 1-D potential energy profile and/or in the particular mechanism of the transition between sites. For instance, models involving traps of random energy depths E_k^t (see Figure 4A) suggest that the rates of transition $W_{k\pm1}$ between sites k and $k \pm 1$ are given by[21−24]

$$W_{k\pm1} = w_0 \exp\left(-\frac{E_k^t}{k_B T}\right) \tag{3}$$

where the preexponential factor is often referred to as the attempt frequency, k_B is the Boltzmann constant, and T is the temperature. In what follows this transport model, invoking out-of-the-well (OUW) transitions, will be called the OUW model (see Figure 4A).

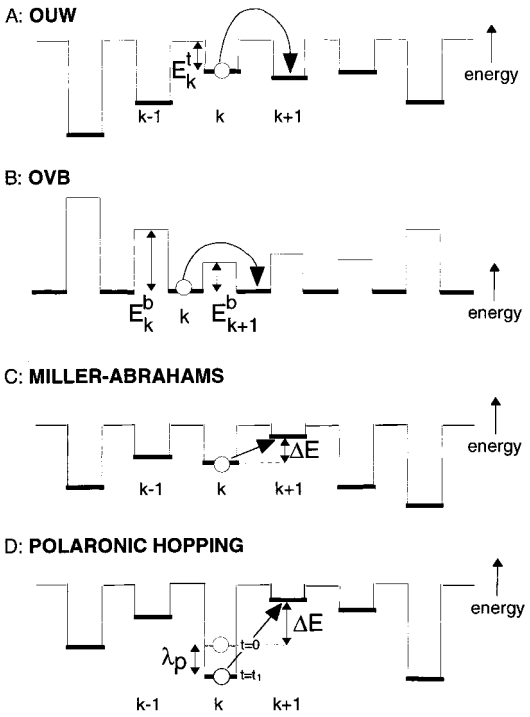

Figure 4. Schematic representation of the energy landscapes used in the different models of charge carrier transport. In parts C and D of Figure 4 the energy difference is equal to $\Delta E = E_{k+1}^{i=s,p} - E_k^{i=s,p}$, with i = s for the Miller−Abrahams transport mechanism in Figure 4C and i = p for the polaronic transport model in Figure 4D.

Another possibility is to approximate disorder by barriers of random heights, E_k^b, between adjacent localization sites (see Figure 4B).[18,20,21,24] The barriers can be overcome either by thermally activated over-the-barrier (OVB) transitions or by tunneling. If only thermally activated jumps occur, the transition rate for a jump over the barrier E_k^b can be written as

$$W_k = w_0 \exp\left(-\frac{E_k^b}{k_B T}\right) \tag{4}$$

Hereafter, this transport model, exploiting eq 4, will be referred to as the OVB model.

Contrary to the above situation, the rate of tunneling transitions through a random barrier depends on the site energies E_k^s explicitly. This case (see Figure 4C) is often treated by using the Miller−Abrahams model[50] for tunneling-assisted hopping (for a review see ref 31). According to ref 50, the rate of tunneling transitions through barriers with a width R can be expressed in terms of the frequency factor ν_0 and the overlap parameter α as

$$W_{k\pm1} = \nu_0 \exp(-2\alpha R) \exp\left[-\frac{E_{k\pm1}^s - E_k^s}{k_B T}\right] \quad \text{for} \quad E_{k\pm1}^s - E_k^s > 0$$

$$= \nu_0 \exp(-2\alpha R) \quad \text{for} \quad E_{k\pm1}^s - E_k^s \le 0 \tag{5}$$

If a charge carrier induces a lattice distortion around itself, the resulting polaron formation should be taken into account (see, for example, ref 51). For polarons with a binding energy λ_p, the transition rate in disordered materials reads (see Figure 4D)

$$W_{k\pm1} = f_0 \exp\left[-\frac{(E_{k\pm1}^p - E_k^p + 2\lambda_p)^2}{8k_B T\lambda_p}\right]$$

$$= f_0 \exp\left(-\frac{\lambda_p}{2k_B T}\right) \exp\left[-\frac{(E_{k\pm1}^p - E_k^p)^2}{8k_B T\lambda_p}\right] \times \exp\left[-\frac{E_{k\pm1}^p - E_k^p}{2k_B T}\right] \tag{6}$$

with f_0 being the temperature-dependent frequency factor for this mechanism.[52]

Calculations of the charge carrier motion with one of the transition rates given above require also a certain distribution function for the energy variable in eqs 3−6. The most common forms of these distributions are the half-Gaussian

$$g(E_k^i) = \frac{2}{(2\pi)^{1/2} E_0^i} \exp\left[-\frac{1}{2}\left(\frac{E_k^i}{E_0^i}\right)^2\right] \quad \text{for} \quad E_k^i \ge 0$$

$$= 0 \quad \text{for} \quad E_k^i < 0 \tag{7}$$

and the exponential

$$g(E_k^i) = \frac{1}{E_0} \exp\left(-\frac{E_k^i}{E_0^i}\right) \quad \text{for} \quad E_k^i \ge 0$$

$$= 0 \quad \text{for} \quad E_k^i < 0 \tag{8}$$

where $E_0^i = k_B T_0^i$ characterizes the degree of disorder for the transport mechanism denoted by *i*. The distributions in eqs 7 and 8 were used for the OUW motion and the OVB jumps. For the Miller−Abrahams and the polaronic mechanism we used a full Gaussian distribution by extending the upper line of eq 7 to include both negative and positive energy values.

Once the transition rate and the distribution function $g(E_k^i)$ are specified, the temperature and temporal behavior of the transport coefficients can be derived by exploiting different analytical approaches.[11−13] In particular, earlier theoretical studies[21,22] suggest that at high temperature $T > T_0^i$, the 1-D transport is Gaussian. The same holds for low temperatures $T < T_0^i$ but only if t is less than the reciprocal of the mean transition rate $1/\langle W\rangle$ obtained by averaging W (from eqs 3−6) over the appropriate energy distribution. Otherwise, i.e., for $t \gg 1/\langle W\rangle$, , the 1-D charge transport becomes dispersive, and the transport coefficients follow a close to power-law time dependence. Thus, the temperature T_0^i can be considered as the point at which the crossover from Gaussian to dispersive transport occurs. It should be mentioned, however, that analytical studies yield expressions for transport coefficients in certain asymptotic limits but fail to provide a detailed description of the 1-D charge transport over the entire time and temperature ranges. In the case where analytical treatments are impossible, computer simulations must be used to investigate this problem.

3.2. Computer Simulations. Computer simulations of the jumplike motion of the charge carriers along 1-D pathways with energy disorder were performed using the Monte Carlo method described earlier.[24,25,53] The transition rates $W_{k\pm1}$ were calculated from eqs 3−6 depending on the transport mechanism assumed. The site energies $E_k^{i=t,s,p}$ or the barrier heights $E_k^{i=b}$ were sampled from the distributions $g(E_k^i)$ using random numbers. The effect of an electric field $\mathbf{F}(\omega,t)$ on the OUW or on the OVB transition rates is taken into account by adding

$\mp(^1/_2)e\mathbf{R}\cdot\mathbf{F}(\omega,t)$ to E_k^t or E_k^b in eqs 3 and 4, respectively. For Miller−Abrahams or polaronic mechanisms, the term $\mp e\mathbf{R}\cdot\mathbf{F}(\omega,t)$ is added to the site energies $E_{k\pm1}^s$ and $E_{k\pm1}^p$ in eqs 5 and 6. The signs account for positive or negative charge carriers. The oscillating electric field is taken as $\mathbf{F}(\omega,t) = \mathbf{F}_0\cos(\omega t + \delta)$ with ω being the frequency and δ being a random phase shift.

To simulate the charge carrier motion along a 1-D pathway, the distribution $p(\Delta t)$ of time Δt spent by the charge carrier at each particular site should be specified. For first-order jump processes, this distribution is given by

$$p(\Delta t) = \exp\left(-\frac{\Delta t}{\tau_k}\right) \tag{9}$$

where the average time τ_k is equal to $(W_{k+1} + W_{k-1})^{-1}$. In the simulations, Δt is sampled from eq 9 by using $\Delta t = -\tau_k \ln(Z)$ with Z being a uniformly distributed random number in the interval $\langle 0,1|$.[54] The probability of a particle to jump from site k to site $k \pm 1$ can be expressed as $P_{k\pm1} = W_{k\pm1}/(W_{k-1} + W_{k+1})$. Another random number Z' is used in order to specify to which neigboring site the particle jumps after a time Δt. If the random number Z' is smaller than or equal to P_{k-1}, the charge carrier is allowed to jump to the site $k - 1$; otherwise, it undergoes a transition to the site $k + 1$.

Similar to the procedure used in refs 24 and 25, the high-frequency ac mobility is calculated according to

$$\mu_{ac}(t) = \frac{1}{e\bar{F}^2\Delta t}\sum_j \Delta U_j(t) \tag{10}$$

where $\Delta U_j(t)$ is the performed work of the charge in the electric field during the time interval Δt and $\bar{F}^2$ is the square of the electric field averaged over Δt. Note that the summation over the index j in eq 10 involves all jumps during the time interval Δt. In the calculations of the ac mobility the columns were assumed to be sufficiently long such that the particle did not reach the end of the column during the simulations.

The above procedure for a single charge carrier is continued until a preset value of t has been reached. Subsequently, a new realization of the energy disorder is generated and the motion of the next charge carrier is simulated in a new Monte Carlo run. The final value of the ac mobility is obtained by averaging over 5×10^4 runs.

In the numerical modeling of the TOF mobility, the length of the column along which a charge carrier moves is taken to be equal to the interelectrode distance used in the experiments. The first disk in the columns is taken to be adjacent to the illuminated electrode, where the charge carriers are produced at time $t = 0$. From this disk the charge carrier, which always has a sign equal to that of the polarity of the adjacent electrode, is not allowed to jump backward into the electrode. The last disk at the end of the column corresponds to the position of the opposite electrode. As soon as a charge carrier arrives at the last disk, immediate neutralization is taken to occur at the electrode surface, and this charge carrier is no longer involved in the simulations.

The jumplike motion of the charge carriers is simulated as a function of time in the same way as described above for the ac mobility by putting $\mathbf{F}(\omega{=}0,t) = \mathbf{F}_0$. Since the time dependence of the position x along the chain is related to the site index in a straightforward manner, the drift velocity of the particles can be obtained from

$$u(t) = \frac{x(t + \Delta t) - x(t)}{\Delta t} \tag{11}$$

The average drift velocity was obtained from several hundred Monte Carlo runs, which was found to be sufficient for convergence of the results. The result of averaging over the Monte Carlo runs was stored as a function of time and corresponds directly to the current decay curve. The transit time of the particles obtained from this curve is used to determine the TOF mobility in a way similar to that applied to the experimental data (see eq 2).

The computational time (CPU) required to perform a simulation of the TOF mobility increases as the temperature decreases, since it becomes more difficult for a charge carrier to overcome higher barriers. At lower temperatures the charge carriers that are adjacent to a higher barrier will make more jumps against the electric field direction before they jump over the barrier toward the opposite electrode. At temperatures below 170 K the amount of CPU time was found to become impracticable.

All simulated results discussed below were obtained by taking for R the characteristic cofacial distance between adjacent aromatic disks equal to 3.5 Å t[10,27,34] and by setting the applied voltage equal to $V = 100$ V in accordance with the TOF experiments. The interelectrode distance was taken to be equal to the experimental value of 31.2 μm. The frequency of the oscillating field was taken to be 30 GHz, which is within the range used in the TRMC experiments.

4. Results and Discussion

In this section we present results of experimental and theoretical studies of charge transport in the columnar liquid crystalline phase of the discotic material T2. The charge carrier mobilities reported here are attributed to holes, since they have been found to be the major charge carriers in TOF measurements on triphenylenes, including the present compound.[4,32,55,56]

4.1. Charge Carrier Mobility. *4.1.1. PR-TRMC Measurements.* Typical PR-TRMC transients are presented in Figure 2. The value of the one-dimensional, intracolumnar mobility, $\sum\mu_{1D} = 3\sum\mu_{PR-TRMC}$, was derived from such transients as described in section 2.2.1. The temperature dependence of $\sum\mu_{1D}$ on cooling from 393 K is shown in Figure 5 (open circles). As can be seen, the mobility is almost independent of temperature and has a value within the range $(1.5 \pm 0.5) \times 10^{-2}$ cm^2 V^{-1} s^{-1} over the entire temperature range investigated. Because the mobility is determined only a few nanoseconds after charge carrier formation, effects due to trapping at domain boundaries or at chemical impurities should be absent. The eventual decay of the transients occurs on a time scale much longer than the pulse width, as shown in Figure 2. The process responsible is thought to be mainly intercolumnar charge recombination, as has been shown to be the case for mesomorphic phthalocyanines.[57]

4.1.2. TOF Measurements. Representative examples of photocurrent transients observed at 358 and 149 K are shown in Figure 3. The transit time indicated in Figure 3A by an arrow could be well resolved at all temperatures between 150 and 400 K. This enables us to use eq 2 for the calculation of the charge carrier mobility μ_{TOF}. The resulting values of μ_{TOF} are plotted at different temperatures in Figure 5 (open triangles).

The data obtained from the TOF experiments show that at close to 400 K the value of μ_{TOF} is very close to the value of the one-dimensional mobility determined in the PR-TRMC measurements. This close agreement at the highest temperatures indicates that the sample used in the TOF measurements

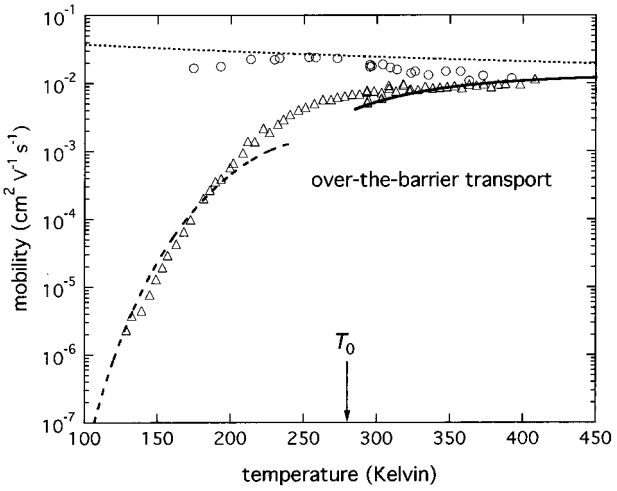

Figure 5. Temperature dependences of the charge carrier mobilities in T2, as measured by the PR-TRMC (circles) and the TOF (triangles) techniques. The lines correspond to analytical evaluations for an exponential distribution of barrier heights (see eq 8), with a width $E_0^b = 0.024$ eV. The ac mobility, calculated from eq 15, is shown by the dotted line. The solid curve is the dc mobility within the high-temperature limit $T > T_0^b = E_0^b/k_B = 280$ K, calculated from eq 14. The dashed line shows the TOF mobility for $T < T_0^b$ evaluated from the transit time, by using eqs A12, 12, and 13.

involves a large monodomain with no grain boundaries over the entire interelectrode distance of 31.2 μm. A monodomain of this extent requires the close to perfect stacking of ca. 10^5 macrocycles! The formation of perfectly oriented columns in the TOF cell has also been reported for hexahexylthiotriphenylene (HHTT)[2,4] and for other triphenylene derivatives.[2,32,37] Apparently, the liquid crystalline phases of triphenylenes are particularly suitable for the formation of orthogonally orientated, extensive monodomains required for successful TOF measurements.

As the temperature is lowered, the value of μ_{TOF} deviates increasingly from the value of $\sum\mu_{1d}$, and at the lowest temperature at which both techniques were used (170 K), the TOF value is more than 2 orders of magnitude lower than $\sum\mu_{1d}$. A substantial further decrease in μ_{TOF} to 2×10^{-6} cm^2 V^{-1} s^{-1} occurs on further lowering the temperature to 130 K.

4.2. Analysis, Simulations, and Comparison with Experimental Results. To elucidate the mechanism of charge carrier transport in the material studied, the experimental results are compared with simulated data obtained for different transport models with the transition rates specified in section 3.1. Our main concern is to find a model that reproduces both the PR-TRMC and the TOF results over the entire temperature range investigated.

Two features of charge carrier transport in 1-D disordered systems are of prime importance for the theoretical analysis of the experimental findings mentioned above. First, the mobility of particles along 1-D pathways with energy disorder is known to decrease with time. Theoretically, such temporal behavior follows from the sublinear dependence of the mean-square displacement on t (see, for example, ref 21) as has been verified by computer simulations.[22,24,25,58] Such a dependence suggests that the difference between the high-frequency and the TOF mobility can be due to the different time scales probed by these two methods. In the PR-TRMC measurements the mobility is determined directly after the 20 ns electron pulse. In contrast, in the TOF measurements the mobility is obtained from the transit time, which ranges from microseconds to milliseconds depending on the temperature of the sample.

Second, the charge carrier mobility in 1-D disordered systems can depend on the frequency of the external electric field (see, for example, refs 24 and 25). This frequency dependence may be another reason for the difference in the results obtained with the PR-TRMC and the TOF techniques. It should be noted, however, that a frequency dependence of the mobility in 1-D disordered systems can be expected only for transport models with asymmetric transition rates;[24,25] i.e., when the rate for a jump from site k to site $k-1$ differs from the rate for a jump to site $k+1$. Such asymmetry is common to the OVB, Miller−Abrahams, and the polaron mechanisms (see eqs 4−6). In contrast, for the OUW mechanism (see eq 3), the transition rates are symmetric, i.e., $W_{k+1} = W_{k-1}$ (see eq 3), and hence, the mobility is frequency-independent.

4.2.1. OUW Model. In the OUW model the diffusion constant[21,22] and the mobility[24] of a charge carrier are time-dependent. As has already been mentioned in section 3.2, the OUW transport undergoes a transition from Gaussian to dispersive transport in the vicinity of the temperature $T_0^t = E_0^t/k_B$ characterizing the width of the distribution of wells over their energy depths; for $T > T_0^t$ the mobility turns out to be independent of time, whereas for $T \leq T_0^t$ it decreases with time. Such behavior allows the conclusion that the distinction in time scales probed by the PR-TRMC and the TOF methods cannot account for the difference between $\sum\mu_{1D}$ and μ_{TOF} as long as T_0^t is assumed to be *lower* than the temperatures used in the experiments. Therefore, in the computer simulations the degree of disorder T_0^t should be in the range between 250 and 320 K, where the distinction between PR-TRMC and TOF results becomes visible. For such a degree of disorder the calculated high-frequency mobility at 20 ns after formation of the charge carrier was found to increase by almost an order of magnitude over the temperature range from 170 to 400 K. The temperature dependence of the mobilty in the OUW model reflects the energy relaxation of the charge carriers.[59] The temperature dependence of the simulated mobility is in disagreement with the exprimental high-freqeuncy mobility, $\sum\mu_{1D}$, which is almost constant from 170 to 400 K (see Figure 5). Hence, the OUW model is not appropriate for an adequate description of the observations.

4.2.2. Miller−Abrahams and Polaronic Models. Within the framework of the Miller−Abrahams (see eq 5) and polaronic transport models (see eq 6), the difference between the PR-TRMC and TOF results can be due to the time and/or the frequency dependence of the mobility,[25] as explained above. The Miller−Abrahams model was applied earlier[27] to describe the TOF results for the D_p phase of T2. The measured TOF mobility values extrapolated to zero external field at temperatures below 250 K could be reproduced by assuming a full Gaussian distribution of the site energies with a width $E_0^s = 0.0482$ eV (corresponding to $T_0^s = 559$ K) and by taking $\nu_0 = 1.2 \times 10^{13}$ s^{-1}. We extended the simulations to higher temperatures and found that the simulated values of the TOF mobility are not in agreement with the experimental observations at nonzero field strength (see Figure 6). In addition for the parameter values from ref 27, we found that the simulated ac mobility shows a temperature dependence, which does not agree with the experimental high-frequency mobility values. The results in Figure 6 show that at $T = 175$ K the simulated ac mobility is about a factor of 5 lower than the measured high-frequency mobility, while at $T = 400$ K the calculated ac mobility is about a factor of 5 higher than the experimental value.

It cannot be excluded that the disagreement between theory and experiments can be reduced in the case of the Miller−

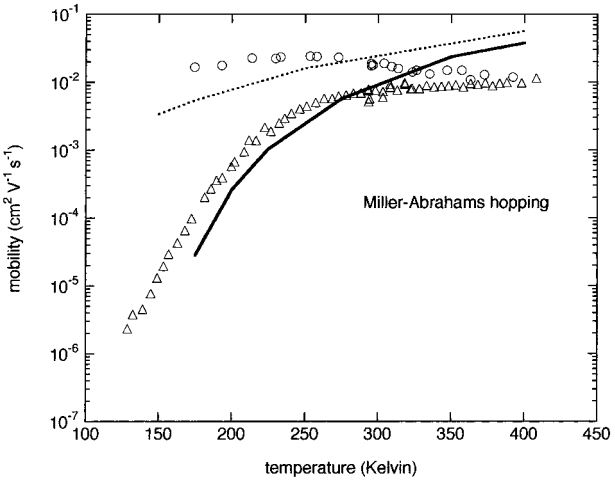

Figure 6. Experimental mobilities of the charge carriers in T2 and the simulated results for the Miller−Abrahams hopping rates (see eq 5) with parameters from ref 27. The experimental PR-TRMC and TOF mobilities are shown by circles and triangles, respectively. The dotted and solid curves correspond to the simulation data on ac and TOF mobilities, respectively.

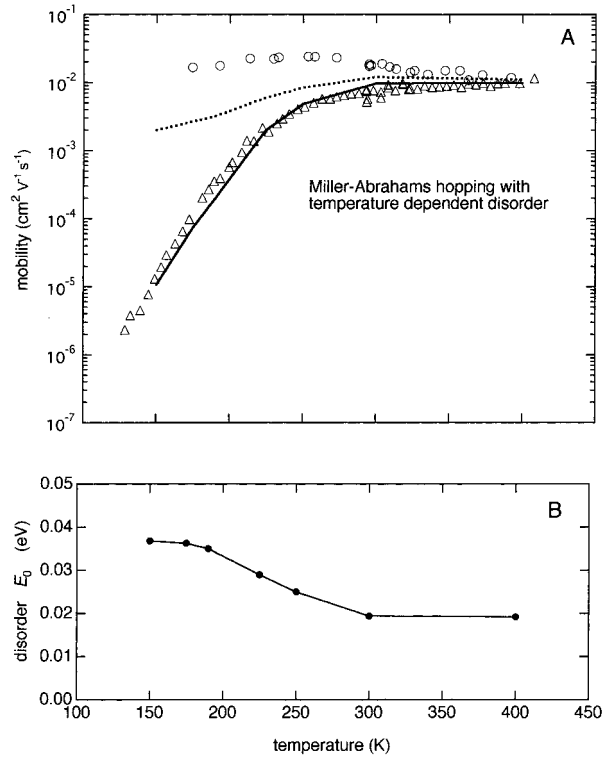

Figure 7. Comparison of experimental mobilities and simulations for Miller−Abrahams charge transport with a temperature-dependent energy disorder. The experimental PR-TRMC and TOF mobilities are shown by circles and triangles, respectively. The dotted and the solid curves are the simulated results, obtained by exploiting the Miller−Abrahams hopping rates (see eq 5) with $\nu_0 = 0.5 \times 10^{12}$ s^{-1} (A) and by assuming a temperature-dependent disorder (B).

Abrahams model by assuming a temperature-dependent disorder.[60] Indeed the Miller−Abrahams model is in reasonable agreement with the experimental TOF results (see Figure 7A) only if the disorder decreases with temperature, as shown in Figure 7B. However, it has been argued that the disorder should increase with temperature.[60] Furthermore, at lower temperatures the simulated ac mobility was found to be smaller than the experimental value by almost 1 order of magnitude (see Figure 7A). All these findings do not corroborate the Miller−Abrahams approach as an adequate description of the charge transport mechanism in the D_p phase of T2.

Another model commonly used to describe charge transport in disordered solids is the polaron model (see eq 6). However, the experimental results could not be reproduced with this model. For a significant polaron binding energy, i.e., $\lambda_p > 0.025$ eV, the experimentally observed plateau for both the $\sum\mu_{1D}$ and μ_{TOF} cannot be obtained. Owing to the factor $\exp[-\lambda_p/(2k_BT)]$ in the transition rate given by eq 6, the simulated mobility shows an increase with temperature above 250 K, in contrast with the experimental data.

4.2.3. OVB Model. In view of the results discussed in sections 4.2.1 and 4.2.2, the model that is still promising for the interpretation of the experimental observations is the OVB model. Contrary to the transport mechanisms considered above, the thermally activated jumps over barriers are not accompanied by energy relaxation of the charge carriers.[24,53,61] In this case the ac mobility can be evaluated by using the Kubo formula,[18,62] while the dc mobility can be obtained from the diffusion coefficient by using the Nernst−Einstein relation[61,62] (see the appendix section).

The asymptotic behavior of the mobility derived by the approximate analytical method outlined in the appendix section is compared with the experimental results in order to obtain values for the parameters needed in the computer simulations. It should be realized that all experimental values of the mobility should be between the bounds predicted by eqs A5 and A8, i.e., the ac mobility for infinite frequency and the dc mobility at infinite time, respectively. For the half-Gaussian distribution (see eq 7), it was found that for any values of the parameters w_0 and T_0^b, the experimental mobilities were not between these bounds over the entire temperature range investigated. Reasoning from this fact, we conclude that the half-Gaussian distribution in eq 7 is inappropriate to describe the spread of the barrier heights in the material investigated.

Turning now to the exponential distribution (see eq 8), we calculate the TOF mobility by using eq A12 with parameters given by[22]

$$\beta = \frac{2T}{T + T_0^b} \tag{12}$$

and

$$\tilde{B} = \frac{4^{\beta-1}\sin^{2-\beta}\left(\frac{\pi\beta}{2-\beta}\right)}{\Gamma(1+\beta)\left(\frac{\pi\beta}{2-\beta}\right)^{2-\beta}} \tag{13}$$

where $\Gamma(z)$ is the gamma function.[63] We found that eq A12 fits very well the experimental TOF mobility below 200 K if $w_0 = 10^{12}$ s^{-1} and $T_0^b = 280$ K (see the dashed line in Figure 5). The current transients simulated with these values for w_0 and T_0^b are shown in Figure 8. The initial decay of the simulated current at 200 K clearly shows the dispersive character of the OVB transport at this temperature. For temperatures above $T_0^b = 280$ K, the current transients exhibit almost no dispersion (see the simulated transient for 300 K in Figure 8). Hence, above 280 K the transit time is determined mainly by the long time limit of the dc mobility. Therefore, the TOF mobility can be very well approximated by the long time limit of the dc mobility (see eq A8). For an exponential distribution

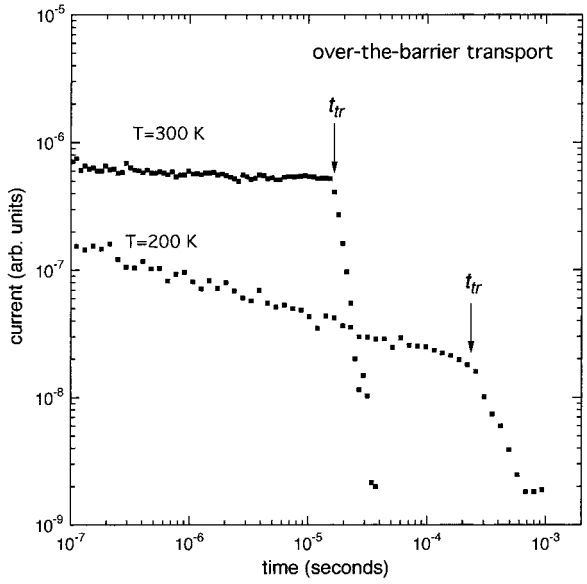

Figure 8. Examples of current transients simulated within the framework of the over-the-barrier transport model for temperatures below and above $T_0^b = 280$ K.

of the barrier heights and $T > T_0^b$, eq A8 gives

$$\mu_{dc}(t\rightarrow\infty) = \frac{ew_0R^2}{k_BT}\left(1 - \frac{T_0^b}{T}\right) \tag{14}$$

As can be seen from the solid line in Figure 5, the analytical results for the TOF mobility above 290 K are in agreement with the experimental values. The ac mobility calculated from eq A5 with an exponential distribution of the barrier heigths is equal to

$$\mu_{ac} = \frac{ew_0R^2}{k_BT}\frac{1}{\left(1 + \frac{T_0^b}{T}\right)} \tag{15}$$

The ac mobility calculated from eq 15 is presented by the dotted line in Figure 5. The results agree well with experimental data of $\sum_i \mu_{1d}$ over the entire temperature range considered.

By use of the values of w_0 and T_0^b from the analytical evaluations, the "exact" mobility values can be obtained from computer simulations as described in section 3.2. Figure 9 shows that the simulated results are in good agreement with the mobilities measured by the PR-TRMC and TOF techniques. Both the analytical consideration and the Monte Carlo simulations prove that the OVB model with an exponential distribution of barrier heights is particularly appropriate for describing the charge transport mechanism. For this model the ac mobility turns out to be time-independent, so the decay of the transients observed in the PR-TRMC experiments (see Figure 2B) can be attributed to the recombination of charge carriers rather than to the time evolution of their mobility.

5. Summary and Conclusions

In the present work we measured the mobility of charge carriers in the hexagonal plastic mesophase of the triphenylene dimer T2 over a temperature range from 130 to 400 K. The results obtained with two complementary techniques, i.e., with the PR-TRMC and TOF methods, are shown to be practically the same above ca. 300 K but become distinct at lower temperatures. Moreover, the mobility $\mu_{PR-TRMC}$ determined in the PR-TRMC experiments was found to be practically temperature-independent, while the TOF mobilities, μ_{TOF}, exhibited a dramatic decrease as the temperature decreases.

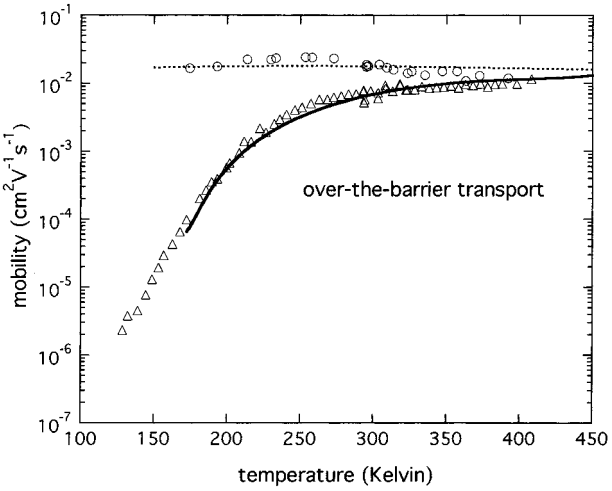

Figure 9. Experimental mobilities of the charge carriers in T2 vs temperature and the Monte Carlo results for the thermally activated hopping over barriers (see eq 4) with an exponential height distribution with a width $E_0^b = 0.024$ eV (see eq 8). Experimental data from the PR-TRMC and the TOF measurements are shown by circles and triangles, respectively. The dotted and solid curves correspond to the simulated results for ac and TOF mobilities, respectively.

To specify the transport mechanism that accounts for the differences observed, we analyzed the experimental data in terms of theoretical models for thermally activated and tunneling-assisted motion of charge carriers along 1-D pathways with energy disorder. Analytical evaluations and computer simulation studies show that the only model consistent with the observations is the model of thermally activated jumps over barriers with random heights. Such incoherent jumplike motion is treated in the present work within the framework of a simple model that involves rectangular random barriers equally spaced along the 1-D pathway. Of course, a more detailed model might include a more realistic potential energy profile, the delocalization of charge carriers over several triphenylene units, effects related to electrode surfaces, and dynamic disorder. Nevertheless, we prefer the simplest model possible, since it is sufficient for understanding the key phenomenon involved. Besides, the available amount of experimental detail does not justify the introduction of additional parameters and assumptions necessarily arising in extended variants of the theoretical framework.

By using the model of thermally activated jumplike motion over random barriers, we have succeeded in describing both the TOF and the PR-TRMC results in terms of an exponential energy disorder with a mean barrier height $E_0^b \approx 0.024$ eV, and hence, $T_0^b = E_0^b/k_B = 280$ K. According to theoretical predictions,[21,23,53] the latter parameter defines the temperature at which the crossover from Gaussian to dispersive transport should be expected. Therefore, it is not surprising that the earlier TOF measurements carried out for triphenylenes with a stable liquid crystalline phase above 300 K did not provide any evidence in favor of 1-D dispersive motion.[2,32,34] In contrast, the temperature range covered in the present work and the time scales probed by the TOF technique are large enough for the change in transport regime as the sample is cooled.

We conclude that the temperature dependence of the mobility observed with the TOF technique can be rationalized in terms of a transition from Gaussian to dispersive transport. The latter transition does not manifest itself in the PR-TRMC experiments, which provide the high-frequency mobility. The high-frequency

mobility probed in these experiments corresponds to almost temperature-independent Gaussian transport, which occurs at short times at all temperatures. This demonstrates that the data obtained with the TOF and PR-TRMC techniques are complementary.

Finally, it should be mentioned that the theoretical results obtained in this work allow several predictions for further numerical and experimental studies. As follows from the theoretical analysis, the ac mobility of charge carriers in discotic liquid crystals should be frequency-dependent, and the TOF mobility is expected to vary with the field strength and with the sample thickness. According to our results, these effects become observable at low temperatures, at which the thermal energy is less than the degree of energy disorder. We expect that experiments to test our predictions might provide additional information about the mechanism of 1-D charge transport in discotic liquid crystals.

Acknowledgment. Dr. C. H. Erdelen (Universität Bayreuth) is acknowledged for the synthesis of the triphenylene material used. This work was supported by the Deutsche Forschungsgemeinschaft (SFB 377) and by The Netherlands Organization for Scientific Research (NWO). Yu.A.B. greatly acknowledges the DFG and the NWO for grants.

Appendix: Analytical Evaluation of the Mobility for Over-the-Barrier Transport

In the case where the 1-D motion of charge carriers is not accompanied by their energy relaxation, analytical evaluations of the mobility can be performed on the basis of general results[11−13,21,22,65] obtained for the over-the-barrier diffusive motion. The evaluations of this quantity for systems with bond disorder, which are beyond the scope of the present work, can be made by employing the results presented in ref 66. Below we evaluate the charge carrier mobility for the over-the-barrier transport, invoking the results of our earlier analytical treatments of 1-D diffusion in disordered systems[21,22] verified by computer simulation studies.[22,58]

According to the Kubo formula, the ac mobility of a particle with charge e is related to the mean squared position $\langle x^2(t)\rangle$ at time t as

$$\mu_{ac} = \frac{e(i\omega)^2}{2k_BT}\int_0^\infty \langle x^2(t)\rangle \exp(-i\omega t)\, dt \qquad (A1)$$

where ω is the radian frequency of the external electric field. Since $\langle x^2(t)\rangle$ can be expressed in terms of the dynamic diffusivity, $D_d(t')$, as

$$\langle x^2(t)\rangle = 2\int_0^t D_d(t')\, dt' \qquad (A2)$$

Equation A1 becomes

$$\mu_{ac} = \frac{e(i\omega)^2}{k_BT}\int_0^\infty \int_0^t D_d(t')\, dt' \exp(-i\omega t)\, dt \qquad (A3)$$

For further evaluations, note that eq A1 is the Laplace transform of the integral over t'. As a consequence, for $s = i\omega$, eq A1 can be rewritten as[64]

$$\mu_{ac} = \frac{es\tilde{D}_d(s)}{k_BT} = \frac{eR^2\tilde{W}(s)}{k_BT} \qquad (A4)$$

with $\tilde{D}_d(s)$ and $\tilde{W}(s)$ being the Laplace transforms of the dynamic diffusivity and the transition rate, respectively. The explicit form of $\tilde{W}(s)$ in different ranges of s values and at different temperatures was specified earlier[21] by using the effective medium approach. In the limit of the high frequency of the external field, i.e., for $\omega > \langle W\rangle$, eq A4 yields

$$\mu_{ac} = \frac{eR^2\langle W\rangle}{k_BT} \qquad (A5)$$

where $\langle W\rangle$ denotes the averaging of the OVB transition rate (see eq 4) over the distribution of barrier heights. Since the mobility in general increases with ω, eq A5 represents the upper limit for the observed mobilities.

Focusing now on the dc mobility, it is useful to mention that eq A1 reduces to the expression for μ_{dc} as ω (and hence s) tends to zero. In this limit the expression for the dc mobility is equivalent to the Nernst−Einstein relation, namely,

$$\mu_{dc} = \frac{e}{k_BT}\lim_{s\to 0}[s\tilde{D}_d(s)] = \frac{eR^2\tilde{W}(s\to 0)}{k_BT} \qquad (A6)$$

Since the asymptotic value of $\tilde{W}(s\to 0)$ in the limit of small s is given by[21,22,58]

$$\tilde{W}(s\to 0) = \frac{1}{\langle 1/W\rangle} \qquad (A7)$$

substitution of eq A7 into eq A6 provides the following expression for the dc mobility

$$\mu_{dc}(t\to\infty) = \frac{e}{k_BT}\frac{R^2}{\langle 1/W\rangle} \qquad (A8)$$

The limit $s \to 0$ used in the derivation of eq A8 corresponds to the long-time limit $t \to \infty$, where the rates for population and depopulation of the localization sites have become equal. Since the dc mobility decreases with time monotonically,[24,25] eq A8 gives the lower bound to the TOF mobility as obtained from the experiments.

To evaluate the TOF mobility μ_{TOF}, we note that for $1/\langle W\rangle \ll t < \langle 1/W\rangle$, the mean-square displacement is given by[22]

$$\langle x^2(t)\rangle = 2R^2\tilde{B}(w_0t)^\beta \qquad (A9)$$

with B and $0 < \beta \le 1$ parameters determined by the explicit form of the barrier height distribution. Equation A9 enables us to write the drift velocity u of charge carriers as

$$u = \mu_{dc}(t_{tr})F = \frac{e\langle x^2(t_{tr})\rangle}{2t_{tr}k_BT}F = \frac{eR^2F}{k_BT}\frac{\tilde{B}(w_0t_{tr})^\beta}{t_{tr}} = \frac{L}{t_{tr}} \qquad (A10)$$

From the last equality in eq A10 one gets

$$w_0t_{tr} = \left(\frac{k_BTL}{eR^2\tilde{B}F}\right)^{1/\beta} \qquad (A11)$$

By substituting this result into the second equality in eq A10 and by using eq A9, we obtain that within the intermediate time range $1/\langle W\rangle \ll t < \langle 1/W\rangle$:

$$\mu_{TOF} = w_0L\left(\frac{eR^2\tilde{B}}{k_BTL}\right)^{1/\beta}F^{(1/\beta)-1} \qquad (A12)$$

References and Notes

(1) Chandrasekhar, S. *Liq. Cryst.* **1993**, *14*, 3.

(2) Adam, D.; Schuhmacher, P.; Simmerer, J.; Häussling, L.; Siemensmeyer, K.; Etzbach, K. H.; Ringsdorf, H.; Haarer, D. *Nature* **1994**, *371*, 141.
(3) Arikainen, E. O.; Boden, N.; Bushby, R. J.; Clements, J.; Movaghar, B.; Woodd, A. *J. Mater. Chem.* **1995**, *5*, 2165.
(4) van de Craats, A. M.; Warman, J. M.; de Haas, M. P.; Adam, D.; Simmerer, J.; Haarer, D.; Schuhmacher, P. *Adv. Mater.* **1996**, *8*, 823.
(5) Markovitsi, D.; Germain, A.; Millié, P.; Gallos, L. K.; Argyrakis, P.; Bengs, H.; Ringsdorf, H. *J. Phys. Chem.* **1995**, *99*, 1005.
(6) Boden, N.; Bissell, R.; Clements, J.; Movaghar, B. *Curr. Sci.* **1996**, *71*, 599.
(7) Bacher, A.; Bleyl, I.; Erdelen, C. H.; Haarer, D.; Paulus, W.; Schmidt, H. W. *Adv. Mater.* **1997**, *9*, 1031.
(8) Bleyl, I.; Erdelen, C.; Etzbach, K. H.; Paulus, W.; Schmidt, H. W.; Siemensmeyer, K.; Haarer, D. *Mol. Cryst. Liq. Cryst.* **1997**, *299*, 149.
(9) Christ, T.; Glüsen, B.; Greiner, A.; Kettner, A.; Sander, R.; Stümpflen, V.; Tsukruk, V.; Wendorff, J. H. *Adv. Mater.* **1997**, *9*, 48.
(10) Zamir, S.; Poupko, R.; Luz, Z.; Huser, B.; Boeffel, C.; Zimmermann, H. *J. Am. Chem. Soc.* **1994**, *116*, 1973.
(11) Alexander, S.; Berlasconi, J.; Orbach, R.; Schnider, W. R. *Rev. Mod. Phys.* **1981**, *53*, 175.
(12) Haus, J. W.; Kehr, K. W. *Phys. Rep.* **1987**, *150*, 263.
(13) Bouchaud, J. P.; Georges, A. *Phys. Rep.* **1990**, *195*, 127.
(14) Scher, H.; Montroll, E. W. *Phys. Rev. B* **1975**, *12*, 2455.
(15) Movaghar, B.; Grünewald, M.; Ries, B.; Bässler, H.; Würtz, D. *Phys. Rev. B* **1986**, *33*, 5545.
(16) Bottger, H. *Hopping Conduction in Solids*; Bottger, H., Bryskin, V. V., Eds.; Academie-Verlag: Berlin, 1985.
(17) Schirmacher, W. *Ber. Bunsen-Ges. Phys. Chem.* **1991**, *95*, 368.
(18) Dyre, J. C. *J. Appl. Phys.* **1988**, *64*, 2456.
(19) Schnörer, H.; Haarer, D.; Blumen, A. *Phys. Rev. B* **1988**, *38*, 8097.
(20) Dyre, J. C.; Jacobsen, J. M. *Chem. Phys.* **1996**, *212*, 61.
(21) Berlin, Y. A.; Burin, A. L. *Chem. Phys. Lett.* **1996**, *257*, 665.
(22) Berlin, Y. A.; Siebbeles, L. D. A.; Zharikov, A. A. *Chem. Phys. Lett.* **1997**, *276*, 361.
(23) Berlin, Y. A.; Burin, A. L. *Chem. Phys. Lett.* **1997**, *267*, 234.
(24) Hilt, O.; Siebbeles, L. D. A. *Chem. Phys. Lett.* **1997**, *269*, 257.
(25) Hilt, O.; Siebbeles, L. D. A. *Chem. Phys.* **1998**, *229*, 257.
(26) Boden, N.; Bushby, R. J.; Clements, J.; Donovan, K.; Movaghar, B.; Kreouzis, T. *Phys. Rev. B* **1998**, *58*, 3063.
(27) Bleyl, I.; Erdelen, C.; Schmidt, H. W.; Haarer, D. *Philos. Mag. B*, submitted.
(28) Bässler, H. *Phys. Status Solidi B* **1981**, *107*, 9.
(29) Scher, H.; Shlesinger, M. F.; Bendler, J. T. *Phys. Today* **1991**, *44*, 26.
(30) Berlin, Y. A. *Mol. Cryst. Liq. Cryst.* **1993**, *228*, 93.
(31) Bässler, H. *Phys. Status Solidi B* **1993**, *175*, 15.
(32) Adam, D.; Closs, F.; T, F.; Funhoff, D.; Haarer, D.; Ringsdorf, H.; Schuhmacher, P.; Siemensmeyer, K. *Phys. Rev. Lett.* **1993**, *70*, 457.
(33) Warman, J. M.; Schouten, P. G. *J. Phys. Chem.* **1995**, *99*, 17181.
(34) Simmerer, J.; Glüsen, B.; Paulus, W.; Kettner, A.; Schuhmacher, P.; Adam, D.; Etzbach, K.-H.; Siemensmeyer, K.; Wendorff, J. H.; Ringsdorf, H.; Haarer, D. *Adv. Mater.* **1996**, *8*, 815.
(35) van de Craats, A. M.; de Haas, M. P.; Warman, J. M. *Synth. Met.* **1997**, *86*, 2125.
(36) van de Craats, A. M.; Schouten, P. G.; Warman, J. M. *J. Jpn. Liq. Cryst. Soc.* **1998**, *2*, 12.
(37) Adam, D.; Schuhmacher, P.; Simmerer, J.; Häussling, L.; Paulus, W.; Siemensmeyer, K.; Etzbach, K. H.; Ringsdorf, H.; Haarer, D. *Adv. Mater.* **1995**, *7*, 276.
(38) Glüsen, B.; Heitz, W.; Kettner, A.; Wendorf, J. B. *Liq. Cryst.* **1996**, *20*, 627.
(39) Schouten, P. G.; Warman, J. M.; de Haas, M. P.; van der Pol, J. F.; Zwikker, J. W. *J. Am. Chem. Soc.* **1992**, *114*, 9028.
(40) Schouten, P. G.; Warman, J. M.; de Haas, M. P. *J. Phys. Chem.* **1993**, *97*, 9863.
(41) Schouten, P. G. Charge Carrier Dynamics in Pulse-Irradiated Columnar Aggregates of Mesomorphic Porphyrins and Phthalocyanines. Thesis, Delft University of Technology, The Netherlands, 1994.
(42) Müller-Horsche, E.; Haarer, D.; Scher, H. *Phys. Rev. B* **1987**, *35*, 1273.
(43) Schmidt, W. F.; Allen, A. O. *J. Phys. Chem.* **1968**, *72*, 3730.
(44) Warman, J. M. In *The Study of Fast Processes and Transient Species by Electron Pulse Radiolysis*; Baxendale, J. H., Busi, F., Eds.; Reidel: Dordrecht, 1982.
(45) Hummel, A. In *The Chemistry of Alkanes and Cycloalkanes*; Patai, S., Rappoport, Z., Eds.; Wiley: New York, 1992.
(46) Infelta, P. P.; de Haas, M. P.; Warman, J. P. *Radiat. Phys. Chem.* **1977**, *10*, 353.
(47) Schouten, P. G.; Warman, J. M.; de Haas, M. P.; van Nostrum, C. F.; Gelinck, G. H.; Nolte, R. J. M.; Copyn, M. J.; Zwikker, J. W.; Engel, M. K.; Hanack, M.; Chang, Y. H.; Ford, W. T. *J. Am. Chem. Soc.* **1994**, *116*, 6880.
(48) Belarbi, Z. *J. Phys. Chem.* **1990**, *94*, 7334.
(49) Hoofman, R. J. O. M.; Siebbeles, L. D. A.; de Haas, M. P.; Hummel, A.; Bloor, D. *J. Chem. Phys.* **1998**, *109*, 1885.
(50) Miller, A.; Abrahams, E. *Phys. Rev.* **1960**, *120*, 745.
(51) Mott, N. F.; Davis, E. A. *Electronic Processes in Non-Crystalline Materials*; Clarendon Press: Oxford, 1979.
(52) Emin, D. *Adv. Phys.* **1975**, *24*, 305.
(53) Berlin, Y. A.; Siebbeles, L. D. A. *Chem. Phys. Lett.* **1998**, *291*, 85.
(54) Press, W. H.; Flannery, B. P.; Teukolsky, S. A.; Vetterling, W. T. *Numerical Recipes*; Cambridge University Press: Cambridge, 1987.
(55) Adam, D.; Haarer, D.; Closs, F.; Funhoff, D.; Siemensmeyer, K.; Schuhmacher, P.; Ringsdorf, H. *Ber. Bunsen-Ges. Phys. Chem.* **1993**, *97*, 1366.
(56) Adam, D. Ph.D. Thesis, University of Bayreuth, 1994.
(57) Schouten, P. G.; Warman, J. M.; Gelinck, G. H.; Copyn, M. J. *J. Phys. Chem.* **1995**, *99*, 11780.
(58) Siebbeles, L. D. A.; Berlin, Y. A. *Chem. Phys. Lett.* **1997**, *265*, 460.
(59) Berlin, Y. A.; Burin, A. L. *Chem. Phys. Lett.*, in press.
(60) Borsenberger, P. M.; Magin, E. H.; van der Auweraer, M.; de Schryver, F. C. *Phys. Status Solidi A* **1993**, *140*, 9.
(61) Baranovskii, S. D.; Faber, T.; Hensel, F.; Thomas, P. *Phys. Status Solidi B* **1998**, *205*, 87.
(62) Kubo, R. *J. Phys. Soc. Jpn.* **1957**, *12*, 570.
(63) Abramowitz, M.; Stegun, I. A. *Handbook of Mathematical Functions*; Dover: New York, 1965.
(64) Erdélyi, A. *Tables of Integral Transforms*; McGraw-Hill: New York, 1954.
(65) Alexander, S.; Bernasconi, J.; Schneider, W. R.; Orbach, R. In *Physcis in One Dimension*; Bernasconi, J., Schneider, T., Eds.; Springer Series in Solid-State Sciences 23; Springer-Verlag: Berlin, Heidelberg, New York, 1981; pp 277−288.
(66) Movaghar, B.; Wurtz, D.; Pohlmann, B. *Z. Phys. B* **1987**, *66*, 523.